PDE-CONSTRAINED OPTIMIZATION FOR NUCLEAR MECHANICS

Yekta Kesenci[1,2],   *Aleix Boquet-Pujadas*[3],   *Emma van Bodegraven*[4],

Sandrine Étienne-Manneville[5],   *Elisabeth Labruyère*[1],   *Jean-Christophe Olivo-Marin*[1]

[1] BioImage Analysis Unit, Institut Pasteur, CNRS UMR 3691, Paris, France.

[2] Université de Paris, Paris, France.

[3] Biomedical Imaging Group, École Polytechnique Fédérale Lausanne, Station 17, 1015 Lausanne, Switzerland.

[4] Department of Translational Neuroscience, Brain Center, UMC Utrecht, Utrecht University, 3584 CG Utrecht, The Netherlands.

[5] Cell Polarity, Migration and Cancer Unit, Institut Pasteur, UMR3691 CNRS, Paris, France.

ABSTRACT

We propose an image based PDE-constrained optimisation framework to compute the dynamical quantities of a cell nucleus undergoing deformation. It allows retrieving the displacement, strain and stress at each pixel of the nuclear domain, as well as the traction force on the boundary. It is based on a mechanical model of the nuclear components and a pair of images documenting the deformation of the cell nucleus. To test our approach, we provide a warping method that produces a second image from an initial one along with the expected mechanical quantities. Both quantitative and qualitative analysis conclude for a significant and consistent improvement of our method over optical flow techniques.

***Index Terms*—** Nuclear mechanics, adjoint method, optical flow

1. INTRODUCTION

The cell nucleus is a complex structure that can transmit force from the cytoskeleton to its interior [1]. Defects in its mechanical properties have been linked to multiple severe diseases, including Hutchinson-Gilford Progeria Syndrome, Emery-Dreifuss muscular dystrophy, and cancer [2]. Being the largest organelle, its stiffness is furthermore a limiting factor for cell deformation and, hence, for 3-D migration in dense environments [3]. Understanding how the cell nucleus deforms after structural change and under constraint is key to pursue further studies in these areas.

The literature provides three types of methods to tackle this challenge for *in vivo* settings. Finite element analysis assumes that the nucleus and its environment follow precise dynamical equations the solution of which can be approximated from their variational form [4]. While the inferred dynamical values are highly accurate, the user is forced to ascribe simplistic geometries to intranuclear and extranuclear elements that cannot account for the complex configuration of nuclear live movement. Morphological methods overcome this issue by deriving strain and force from the analysis of the shape of
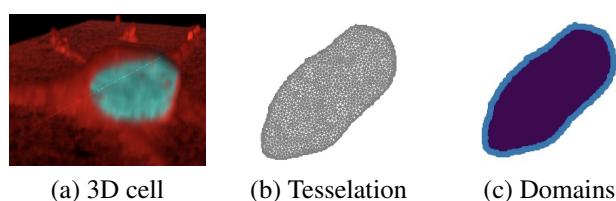

(a) 3D cell   (b) Tesselation   (c) Domains

Fig. 1: (a) 3D image of the nucleus (blue) and of its cytoplasm (red). (b) Mesh generation. (c) Lamin domain (light blue) and chromatin domain (dark blue). Mesh is coarser for visibility.

the nuclear surface [5], but intranuclear movement – which is of foremost importance if one is to consider the role of chromatin in overall nuclear mechanics – evades their investigation. Optical flow methods take both the shape of the nucleus and intranuclear movement into account [6]. Such approaches generally require two images of the nucleus, one before deformation and the other after, and define with them a functional to minimize that contains data and regularization terms. Accuracy can be improved by choosing the right regularisation parameters, but these generally overlook mechanical properties such as stiffness. Furthermore, these methods generally consider the entire image, but we would like to constrain the mechanical analysis only to the nuclear domain. We demonstrate that a combination of optical flow and mechanical modeling allows to unite the strengths of these two approaches.

Following the work of [7], we propose a PDE-constrained optimisation framework to compute all the mechanical quantities of interest in the study of nuclear deformation, namely: displacement, strain and stress at each of the pixels inside, and the traction force on the boundary. First, a displacement field is derived using optical flow [8]. Then an inverse optimization problem is formulated: it seeks to find those displacements that come closest to the computed field while also abiding by the dynamical model of the nucleus. We solve it by resorting to the theory of optimal control [9]. Using finite differences, we retrieve from this solution the strain and stress fields, as well as the traction force on the boundary. Simulating traction over the nuclear boundary, we warp a 2D image of a nucleus

ICIP 2022

to create a second one after deformation. These two images are used to test the validity of our method: we show that our reconstruction not only faithfully reproduces the mechanical quantities guiding deformation, but that it distinctly surpasses the results we would get from optical flow techniques alone.

2. DYNAMICAL MODEL OF THE NUCLEUS

Building a comprehensive model that would account for all nuclear components and all protein interactions such as the LINC complex is still out of reach. Yet research over the last decades agree its overall mechanical response relies mostly on the properties of two of its constituents [2]: the nuclear lamina and the chromatin. The nuclear lamina is a $10 - 100$ nm meshwork that underlies the nuclear envelope. The chromatin fills the nuclear interior, which is about $10\ \mu m$ thick. Both domains are linked through molecular interactions. We therefore model them as a lamin shell wrapping the chromatin domain without sliding on it (Fig 1.c).

In the remaining of this paper, we will assume that lamina and chromatin are both continuous media. This assumption holds true at the microscopic level, where most confocal microscopes operate, but would need to be reevaluated if one were to work with smaller scales, where the meshwork structure of the lamin and the fractal-like configuration of the chromatin might be more relevant. Suppose now the nucleus encompasses a domain $\Omega \subset \mathbb{R}^n$, where $n \in \{2,3\}$. We define lamin as the boundary of this domain and chromatin as its complement, i.e. as the whole domain except the boundary. The literature concurs on assigning either of two main mechanical models to them: elastic or viscoelastic. We will assume both domains follow an isotropic linearly elastic model, albeit of different stiffness; this is a good approximation at large timescales and small deformations, two regimes that well fit our biological data. We suppose here that nuclear deformation happens only from external mechanical constraints and not from volumic forces as to model mechanotransduction. The framework we propose applies nonetheless to any other kind of mechanical model. This settled, we can establish the equations ruling the nuclear domain Ω:

$$
\begin{cases}
\nabla \cdot \sigma = 0 & \text{in } \Omega, \\
\sigma(u) := \lambda \operatorname{tr}(\varepsilon(u))I + 2\mu\varepsilon(u) & \text{in } \Omega, \\
\varepsilon(u) := \frac{1}{2}(\nabla u + \nabla u^T) & \text{in } \Omega, \\
\lambda = \lambda_l,\ \mu = \mu_l & \text{on } \Gamma, \\
\lambda = \lambda_c,\ \mu = \mu_c & \text{in } \Omega \setminus \Gamma \\
u = g & \text{on } \Gamma.
\end{cases}
\tag{1}
$$

The first two equations are the balance and constitutive equations, the third defines a compatible strain. $u \in L^2(\Omega)$ is the displacement field, $\varepsilon, \sigma \in M_{n,n}(\Omega)$ the second order strain and stress tensors, respectively, and g the displacement on the boundary. The functions λ and μ are the Lamé parameters that take different values specific to the chromatin

and the lamin domains. Their dimension is that of stress. The first one becomes larger as the compressibility of the material increases, whereas the second rules the material behaviour in the face of shear deformation. Both can be computed from Young's modulus and Poisson's ratio, two constants more readily available in the literature.

3. PDE-CONSTRAINED OPTIMIZATION

Optical flow is a generic term for a set of methods to compute velocity fields between a pair of images of a moving object. The seminal Horn-Schunck method (HS) assumes three hypothesis: brightness constancy, small displacements and regularity of the solution [8]. Immunofluorescence microscopy employs biological markers that yield texturised fluorescence images that agree with the brightness constancy assumption. While photobleaching decreases the intensity over time, it does so homogeneously and would not affect the framework after proper normalization. The small displacement assumption is likewise fulfilled here, the confocal microscope being faster than the time scale of the movement, but could otherwise be tackled with a multiresolution scheme.

Together, the three assumptions assert that the velocity v at each pixel in the first image will be obtained through the resolution of the following problem:

$$
\arg\min_v \int_{\Omega_I} \left(\frac{\partial I}{\partial t} + v \cdot \nabla I \right)^2 + \alpha ||\nabla v||^2,
\tag{2}
$$

where Ω_I is the domain of the image function I and α is a regularization constant. This problem is in turn solved using an iterative scheme on the Euler-Lagrange equations. Starting with the solutions computed with optical flow, one can differentiate the velocity to compute the strain, then the stress, and then the traction vector over the boundary. But we wouldn't profit from the information we might get from the mechanical knowledge we hold on the nucleus: there is a better strategy.

One would like to choose, among all the displacement fields, the 'closest' to the one computed with optical flow that still obeys the dynamical equations stated in the previous paragraph. We thus propose an alternative problem. Noting $\hat{u}$ the solution computed from (2):

$$
\arg\min_{u,g} \quad J(u,g) := \int (u - \hat{u})^2 + \beta \left(\nabla g \cdot n_\perp \right)^2 d\Omega,
$$
$$
\text{s.t.} \quad \text{eq. (1)}
\tag{3}
$$

where g is the boundary displacement, here acting as a control variable, and $n_\perp$ the boundary's tangent. The gradient of the displacement is again penalized to ensure regular solutions, which otherwise would lead to spurious values of the strain and the stress.

Using the finite element method, we compute for each boundary condition g the solution u of the equations. The implicit function theorem allows us to consider u as a function

of g, and therefore the functional J as a function of g alone. This means that we can formulate our constrained problem into an unconstrained one. It is then solved through the use of a quasi-Newton gradient descent algorithm that seeks to find the boundary condition g that minimizes the prescribed functional. In order to avoid large computations, we compute the gradient using the adjoint method [9].

4. RESULTS

Optical flow methods enjoy a set of carefully crafted tests to assess their performance. Mechanobiology lacks such database, so one must design their own ground truth to compare the accuracy of what they set forth. We propose a warping strategy that will give a pair of images, one before deformation and the other after, along with the ground truth displacement field, strain and stress tensors, and traction boundary, that underly this deformation. We start with an image of a nucleus issued from a confocal microscope (Fig. 1.a). We segment it using k-means hierarchical clustering followed by active contours. We apply Delaunay's algorithm [10] on the resulting contour to create a mesh of the nuclear domain (Fig. 1.b). We define on this mesh the forward problem in variational form, which can be derived either by minimizing the Hellinger-Reisner energy potential of isotropic linear elasticity or by differentiation of the provided dynamical equations with Green's theorem:

$$\begin{cases} a(u,w) = L(w), \\ a(u,w) := \int \sigma(u;\lambda,\mu) : \varepsilon(w) \, d\Omega, \\ L(w) := \int T \cdot w \, d\Gamma_T. \end{cases} \quad (4)$$

Here Γ_T is the subdomain of the nuclear boundary where we will be simulating the tension induced by a micropipette. $u \in H^1(\Omega)$ is the trial function and $w \in \{v \in H^1(\Omega)|v = 0 \text{ on } \Gamma\}$ is the test function. Given the values of T and of the Lamé parameters, we use the finite element method to compute the "ground truth" displacement u (Fig. 2.d.) and warp our initial image using an order 2 spline interpolation to produce an image of the deformed nucleus (Fig. 2.a, 2.b). We apply HS to these two images (Fig. 2.e), then solve problem (3) thanks to the dolfin adjoint library [11](Fig. 2.f). Derivation allows retrieving the hydrostatic strain $\varepsilon_h = \text{tr}(\varepsilon)$, along with the von Mises stress $\sigma_M = \sqrt{\frac{3}{2}s : s}$, where $s = \sigma - \frac{1}{3}\text{tr}(\sigma)I$, (Fig. 2.g-j) and the traction boundary (Fig. 2.k-m).

Error norms and constants. We measure the accuracy of our method with the root mean square error (RMSE) of the hydrostatic strain and of the von Mises stress, normalized over the range, along with the ratio of the norm of the computed boundary traction over the norm of the true traction. We suppose a Young modulus of 250 Pa and a Poisson ratio of 0.3 for the chromatin, and that the lamin is 5 times stiffer. To produce higher deformations, we extend the traction domain to the bottom of the nucleus. We compare the accuracy of our
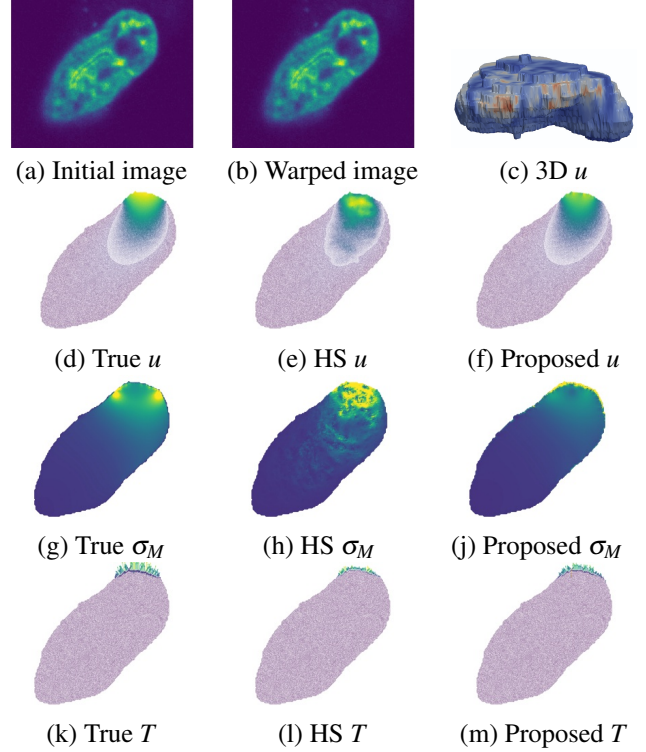

(a) Initial image (b) Warped image (c) 3D u

(d) True u (e) HS u (f) Proposed u

(g) True σ_M (h) HS σ_M (j) Proposed σ_M

(k) True T (l) HS T (m) Proposed T

Fig. 2: Comparison of the mechanical quantities of interest (displacement, stress, traction) obtained using HS and our method in regard of the ground truth quantities obtained from finite element analysis. Here $||T|| = 2.5$ Pa and lamin is 5 times stiffer than chromatin.

method over some of the most popular optical flow methods in biology: Horn Schunck (HS) [8], TV-L1 [12], large displacement optical flow (LDOF) [13], iterative Lukas-Kanade (ILK) [14]. We choose the regularization parameters of all these methods according to the L-curve criterium.

First experiment. We compare the variation in accuracy for increasing values of the boundary traction $||T|| \in \{0.25, 0.375, ..., 0.75\}$ Pa (Table 1). While excellent at computing the strain and the stress, optical flow methods prove less accurate and less robust against varying deformations compared to our method (Fig. 3.a-c). Furthermore they outright fail at retrieving the traction, despite good stress recovery. On the contrary, our method is relatively accurate, although it does suffer from deviations with increasing traction. We believe this can be overcome by using non-linear elasticity equations to account for larger deformations.

Second experiment. We fix the initial traction to 2 Pa and compute the accuracies for varying values of the Poisson ratio of the lamin $v_{lamin} \in \{0.30, 0.34, ..., 0.48\}$ (Table 1). Again, our method proves consistently more accurate and robust. This is especially true when the lamin becomes incompressible: while our method's stress accuracy remains stable, the accuracy of optical flow methods plunges (Fig 3.d.).
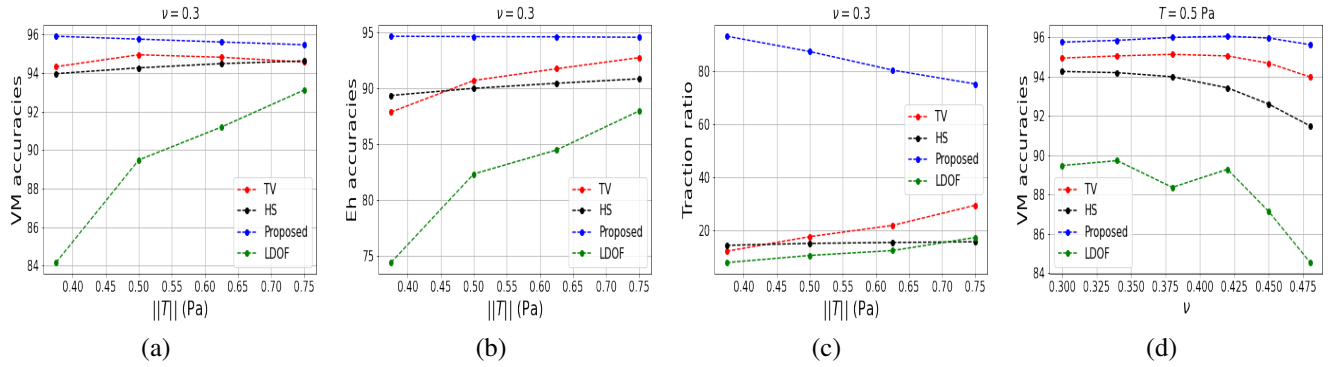
2194

Fig. 3: Evolution of the accuracies of the von Mises stress, the hydrostatic strain and the traction boundary of our method against the three top performing optical flow methods.

Experiment 1	NRMSE σ_M	NRMSE E_{hyd}	Traction ratio	Experiment 2	NRMSE σ_M	NRMSE E_{hyd}	Traction ratio
Proposed	**95.67 ± 0.16**	**94.60 ± 0.03**	**84.16 ± 6.82**	**Proposed**	**95.86 ± 0.14**	**95.10 ± 0.37**	**88.25 ± 2.45**
TV-L1	94.65 ± 0.23	90.76 ± 1.81	20.39 ± 6.31	TV-L1	94.80 ± 0.39	91.38 ± 0.55	13.84 ± 2.35
ILK	67.86 ± 1.17	41.78 ± 2.3	4.92 ± 0.29	ILK	59.09 ± 7.05	45.03 ± 3.57	3.40 ± 0.83
LDOF	89.48 ± 3.33	82.31 ± 4.97	12.13 ± 3.45	LDOF	88.09 ± 1.80	84.14 ± 1.33	8.04 ± 1.53
HS	94.33 ± 0.24	90.16 ± 0.55	15.25 ± 0.50	HS	93.32 ± 0.99	90.74 ± 0.59	11.35 ± 2.81

Table 1: Mean and standard deviation of the accuracy over the varying constants.

5. CONCLUSION

We proposed a PDE-constrained optimization framework that allows the retrieval of mechanical quantities from images of a nucleus undergoing deformation. For now, only optical flow techniques are capable of similar feats, but our method proves more accurate and more stable by including mechanical information into the variational problem. We also showed that optical flow fails at recovering the traction, and that our method offers a convincing alternative. This technique has already allowed us to recover live nuclear deformations (Fig. 2c) at the accuracy required to distinguish the contribution of different proteins involved in cell migration.

6. ACKNOWLEDGMENTS

7. REFERENCES

[1] J. Lammerding, "Mechanics of the nucleus," *Comprehensive physiology*, vol. 1, no. 2, p. 783, 2011.

[2] C. M. Hobson and A. D. Stephens, "Modeling of cell nuclear mechanics: Classes, components, and applications," *Cells*, vol. 9, no. 7, p. 1623, 2020.

[3] A. L. McGregor, C.-R. Hsia, and J. Lammerding, "Squish and squeeze—the nucleus as a physical barrier during migration in confined environments," *Current opinion in cell biology*, vol. 40, pp. 32–40, 2016.

[4] X. Cao, E. Moeendarbary, P. Isermann, *et al.*, "A chemomechanical model for nuclear morphology and stresses during cell transendothelial migration," *Biophysical journal*, vol. 111, no. 7, pp. 1541–1552, 2016.

[5] I. D. Estabrook, H. R. Thiam, M. Piel, and R. J. Hawkins, "Calculation of the force field required for nucleus deformation during cell migration through constrictions," *PLoS computational biology*, vol. 17, no. 5, e1008592, 2021.

[6] Q. Gao and K. Rohr, "A global method for non-rigid registration of cell nuclei in live cell time-lapse images," *IEEE Transactions on Medical Imaging*, vol. 38, no. 10, pp. 2259–2270, 2019.

[7] A. Boquet-Pujadas, T. Lecomte, M. Manich, *et al.*, "Bioflow: A non-invasive, image-based method to measure speed, pressure and forces inside living cells," *Scientific reports*, vol. 7, no. 1, pp. 1–16, 2017.

[8] B. K. Horn and B. G. Schunck, "Determining optical flow," *Artificial intelligence*, vol. 17, no. 1-3, pp. 185–203, 1981.

[9] P. Lions, "Optimal control," in *ICIAM 91: Proceedings of the Second International Conference on Industrial and Applied Mathematics*, SIAM, vol. 61, 1992, p. 182.

[10] M. Alnæs, J. Blechta, J. Hake, *et al.*, "The fenics project version 1.5," *Archive of Numerical Software*, vol. 3, no. 100, 2015.

[11] S. K. Mitusch, S. W. Funke, and J. S. Dokken, "Dolfin-adjoint 2018.1: Automated adjoints for fenics and firedrake," *Journal of Open Source Software*, vol. 4, no. 38, p. 1292, 2019.

[12] J. S. Pérez, E. Meinhardt-Llopis, and G. Facciolo, "Tv-l1 optical flow estimation," *Image Processing On Line*, vol. 2013, pp. 137–150, 2013.

[13] T. Brox and J. Malik, "Large displacement optical flow: Descriptor matching in variational motion estimation," *IEEE transactions on pattern analysis and machine intelligence*, vol. 33, no. 3, pp. 500–513, 2010.

[14] A. Plyer, G. Le Besnerais, and F. Champagnat, "Massively parallel lucas kanade optical flow for real-time video processing applications," *Journal of Real-Time Image Processing*, vol. 11, no. 4, pp. 713–730, 2016.